Metal-insulator transition in the Hartree-Fock phase diagram of the fully polarized homogeneous electron gas in two dimensions

B. Bernu,[1] F. Delyon,[2] M. Duneau,[2] and M. Holzmann[1,3]
[1]*LPTMC, UMR 7600 of CNRS, Université P. et M. Curie, 75752 Paris, France*
[2]*CPHT, UMR 7644 of CNRS, École Polytechnique, 91128 Palaiseau, France*
[3]*LPMMC, UMR 5493 of CNRS, Université J. Fourier, 38042 Grenoble, France*
(Received 9 April 2008; revised manuscript received 20 October 2008; published 10 December 2008)

We determine numerically the ground state of the two-dimensional fully polarized electron gas within the Hartree-Fock approximation without imposing any particular symmetries on the solutions. At low electronic densities, the Wigner crystal solution is stable, but for higher densities (r_s less than ~ 2.7) we obtain a ground state of different symmetry: the charge density forms a triangular lattice with about 11% more sites than electrons. We prove analytically that this conducting state with broken translational symmetry has lower energy than the uniform Fermi-gas state in the high-density region giving rise to a metal to insulator transition.

DOI: 10.1103/PhysRevB.78.245110 PACS number(s): 71.10.Ca, 71.10.Hf, 71.30.+h

I. INTRODUCTION

The two-dimensional homogeneous electron gas is one of the fundamental models in condensed-matter physics. Despite its simplicity—the system consists of electrons interacting through a $1/r$ potential to which a uniform positive background is added for charge neutrality—the phase diagram at zero temperature is nontrivial.[1–3] In general, it is given in terms of the dimensionless parameter $r_s=1/\sqrt{\pi n a_B^2}$, where n is the electronic density and $a_B=\hbar^2/(me^2)$ the Bohr radius (see Sec. IV for notations and units). At low density (large r_s), the potential energy dominates over the kinetic energy and the system forms a triangular lattice, the Wigner crystal (WC), whereas in the high-density region ($r_s \to 0$) the kinetic energy favors a uniform Fermi-gas (FG) phase[1] (the simplest state given as the determinant of the plane waves with wave vector $\mathbf{k}$ of modulus smaller than k_F). The energy of the FG is known analytically. Already Wigner[4] argued that the unpolarized FG is unstable even in the limit $r_s \to 0$. Later, Overhauser[5] claimed the instability of the unpolarized WC with respect to spin-density waves, even within the Hartree-Fock approximation (HF). It has further been conjectured that the Coulomb potential prevents any first-order transition between the WC and a FG.[6] Despite these rather general instability theorems, there are few quantitative calculations of the true ground state of the electron gas within HF.[7] A previous HF study[8] of the two- and three-dimensional electron gas compares the FG energy with the energy of various states with imposed crystal symmetries. For the polarized two-dimensional gas, they find lower energies for a crystal for r_s larger than 2. Only recently an unrestricted HF study of the unpolarized three-dimensional electron gas was performed which proposes a more complicated structure of a ground state with spin-density waves in the high-density region.[9]

Indeed, establishing the precise HF phase diagram of the electron gas influences the correlation energy estimations, since by definition the many-body correlation effects must be evaluated with respect to the true HF ground state. Further, even in more advanced techniques, the antisymmetry of the wave functions is in general provided by a single Slater determinant.

In the present study, we consider the fully polarized two-dimensional electron gas, analytically and numerically. Section II summarized our numerical results. At low densities, $r_s \gtrsim 2.7$, our simulations always lead to a WC. For higher densities and large enough number of electrons, N, the solution is neither a FG nor a WC: the density modulation corresponds to a partially occupied crystal of different symmetry compared to the WC phase. As the number of sites is larger than N, we refer to this solution as a metallic phase. Details of our numerical methods are given in Sec. III.

In Sec. IV we remind some definitions and notations particularly used in the following. Section V is devoted to derive rigorous analytical upper bounds on the energy of the metallic phase. These bounds are obtained in the limit $r_s \to 0$ where the calculation is simplified by the long-range behavior of the interaction potential. In the conclusion, Sec. VI, we briefly summarize the results of the paper and discuss their relevance.

The HF solutions discussed in this paper within the HF approximation open a perspective for the qualitative understanding of the experimental observed metal to insulator transition[10] and should be considered in studies beyond the HF approximation. The possibility that the experimental findings are driven by interaction effects—and not by disorder—was recently addressed in Refs. 11 and 12 considering an extended Hubbard model.

II. NUMERICAL RESULTS

The N-body Hamiltonian, $H=K+V$, contains the kinetic energy K and the $1/r$-periodic Coulomb potential V where a uniform positive charge background is subtracted. Within the HF approximation, the search of the true ground state of the quantum many-body system is reduced to the simpler problem of finding the lowest energy states in the subset of the Slater determinants [see Eq. (10)]. Let $\Phi=\psi_1 \wedge \cdots \wedge \psi_N$ be the Slater determinant associated with the single-particle states $\{\psi_i\}$ and $E(\psi_1, \psi_2, \ldots, \psi_N)$ the corresponding energy expectation value.

By a kind of descent method described in Sec. III, we numerically study systems with up to 500 electrons at den-

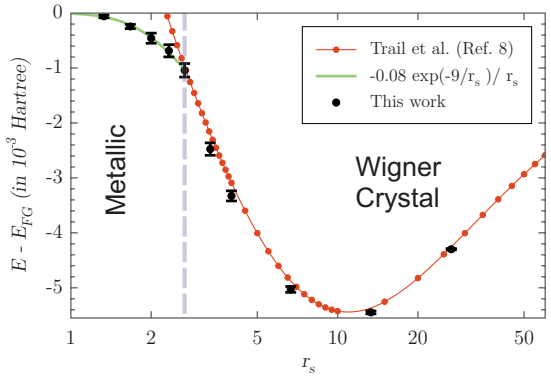

FIG. 1. (Color online) Extrapolated energies $E_\infty - E_{\mathrm{FG}}$ (milli-Hartree units) versus r_s. Points with error bars: present calculations, full line (red): data of Ref. 8, full line (green): fit to present results for ($r_s \lesssim 2.7$), vertical dash line (blue): $r_s \sim 2.7$.

sities corresponding to $r_s=1$ up to $r_s=30$. Since we expect the electrons to crystallize on a triangular lattice at low densities, we choose periodic conditions compatible with this geometry. Thus, the unit cell of the periodized system is given in terms of two vectors $\{\mathbf{L}_1,\mathbf{L}_2\}$ of length L and with an angle of 60° between both; the volume of the unit cell is $\Omega=L^2\sqrt{3}/2$. We have restricted our study to system sizes which are compatible both with the triangular lattice and with a closed-shell occupation in k space. Any triangular crystal with unit-cell vectors $\{\mathbf{e}_1,\mathbf{e}_2\}$ is compatible with the boundary conditions if it satisfies $\mathbf{L}_1=l\mathbf{e}_1+m\mathbf{e}_2$ and $\mathbf{L}_2=-m\mathbf{e}_1+(l+m)\mathbf{e}_2$, where (l,m) are two non-negative integers. The number of sites of the lattice is given by $N_c=\det(\mathbf{L}_1,\mathbf{L}_2)/\det(\mathbf{e}_1,\mathbf{e}_2)=l^2+m^2+lm$.

In Fig. 1, we report the energies of the obtained HF ground state $E_\infty(r_s)$, extrapolated to the thermodynamic limit, as a function of r_s. In the low-density region, for $r_s>3$, we obtain good agreement with the results of Trail *et al.*,[8] which imposed a ground-state build as a complete band of Bloch wave functions of the triangular WC lattice. But for smaller r_s we find lower energies which remain also below the FG energy down to $r_s=1$.

Figure 2(a) shows the typical charge density for $r_s \approx 3$. In this case we have a triangular lattice with exactly N sites. Figure 2(c) shows the Fourier transform of the charge density. The support of the Fourier transform is the sixfold star corresponding to the triangular lattice of the charge density with $N_c=N$.

For $1<r_s<2.7$, we find different kind of ground states [see Fig. 2(b)]: the support of the Fourier transform [see Fig. 2(d)] is still a sixfold star corresponding to a triangular lattice, but this triangular lattice has a number of sites N_c larger than N. The system lowers its energy by delocalizing the electrons on a denser lattice with more sites than electrons (Fig. 2). This denser lattice is characterized by integral numbers (l',m') different from the WC lattice (l,m). For some system sizes N, the maxima of the Fourier transform correspond to various couples of $\{l',m'\}$ leading to different number of lattice sites, $N_c=l'^2+m'^2+l'm'$. In any case, the system looks like a periodic crystal with an incomplete band in contrast to the WC solutions of fully occupied bands, studied in Ref. 8. We refer to this solution as the metallic phase. However, as r_s approaches zero, the energy gain of this metallic crystal compared to the FG gets tinier. At the same time, N_c is either constant or increases when r_s decreases (apart for a few exceptions). At $r_s<1$, the FG solution is stable for our finite system sizes ($N \leq 500$).

Now we would like to understand the nature of the Slater determinants in the metallic phase. A Slater determinant is obtained as a set of N orthonormal single-particle wave functions ψ_i. Only the space generated by the ψ_i's is relevant, and in order to understand the numerical results we need to choose a canonical representation of the ψ_i's.

Let $\{\phi_i\}_{i=1\ldots N}$ be a basis corresponding to some indexation of the plane waves associated to the wave vectors $\mathbf{k}_i$ of the Fermi sphere. As r_s is small, the space generated by the ψ's becomes close to the space generated by the ϕ's. Let M be the square matrix defined by $M_{ij}=\langle\phi_i|\psi_j\rangle$ which measures the overlap of the two Slater determinants. The singular

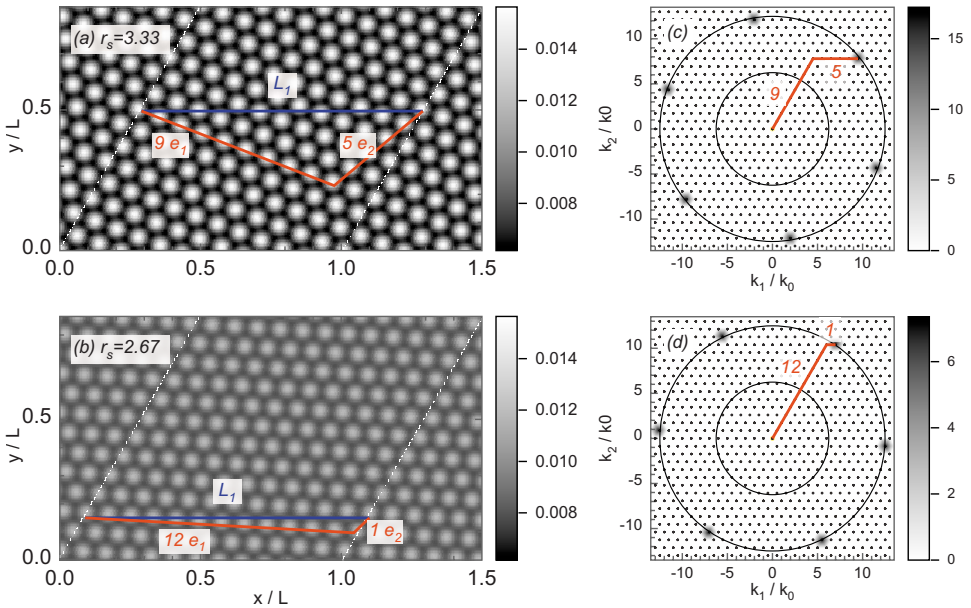

FIG. 2. (Color online) Left: charge density $\rho(\mathbf{r})/\langle\rho\rangle-1$, with $\rho(\mathbf{r})=\Sigma_{i=1}^{N}|\varphi_i(\mathbf{r})|^2$. Right: $\tilde{\rho}(\mathbf{k})$, the Fourier transform of the charge density, where $\tilde{\rho}(0)=N$ has been removed. The grid points are those compatible with the periodic conditions. Top: the number of maxima is $N_c=9^2+5^2+9\times5=151$. Bottom: the number of maxima is $N_c=12^2+1^2+12\times1=157$. Gray levels corresponds to the same density in both figures. Colored lines correspond to $\mathbf{L}_1=l\mathbf{e}_1+m\mathbf{e}_2$, where the numbers stand for l, m (see text).

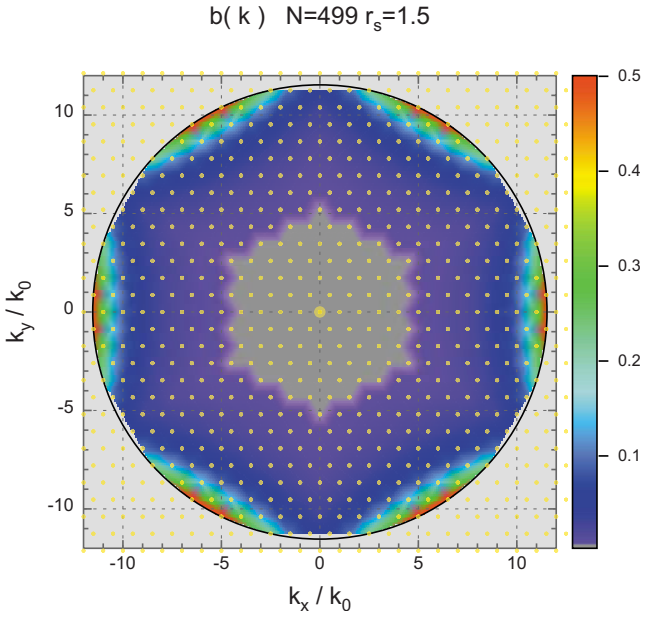

FIG. 3. (Color online) Numerical values of b_k for 499 electrons in two dimensions at $r_s=2$.

value decomposition (SVD) of M is $M=U\sigma V$, where U and V are unitary matrices and σ is a diagonal positive matrix. Then the orthonormal set $\{\psi_i'\}_{i=1\ldots N}$ defined by

$$\psi_i' = \sum_k \overline{UV}_{ik}\psi_k \tag{1}$$

is a basis of Span$(\{\psi_i\})$ close to the basis $\{\phi_i\}_{i=1\ldots N}$ of Span$(\{\phi_i\})$ in the sense that $\langle\phi_i|\psi_j'\rangle=(\overline{U}\sigma U^T)_{ij}\approx\delta_{ij}$ as soon as σ_i's are close to 1. From now on, we assume that the single-particle wave functions, ψ_i, have been chosen in this way.

Thus if r_s is not too large, ψ_i is close to ϕ_i (at least for i associated to a wave vector not too close to the Fermi surface), that is, $\psi_i(\mathbf{k}_i)$ is close to one. Thus, the largest amplitude of $\psi_i(\mathbf{k})$ is for $\mathbf{k}=\mathbf{k}_i$, and Fig. 3 represents the next largest amplitude of ψ_i, that we denote $b_{\mathbf{k}_i}$, for 499 electrons at $r_s=2.7$ in two dimension (2D).

For $|\mathbf{k}_i|\approx k_F$, ψ_i has essentially only two nonzero components: one at $\mathbf{k}=\mathbf{k}_i$ and the other one b_{k_i} at the vector $\mathbf{k}=\mathbf{k}_i+\mathbf{q}_i$, where $\mathbf{q}_i$ is the vector of the sixfold star of Fig. 2(d) such that $\mathbf{k}$ is close to the Fermi surface. This condition can only be satisfied for a set of $\mathbf{k}_i$ closed to a sixfold star as we see on Fig. 3.

One can understand why metallic states should exist at small r_s in the thermodynamic limit. Let us replace a plane-wave state $\mathbf{k}$ of the FG ($\|\mathbf{k}\|\leq k_F$) by a superposition of two plane waves with wave vectors $\mathbf{k}$ and $\mathbf{k}+\mathbf{q}$ ($\|\mathbf{k}+\mathbf{q}\|>k_F$). Choosing $\mathbf{q}$ on the sixfold star of a triangular lattice we certainly obtain a gain in potential energy. The increase of kinetic energy is minimized if $\|\mathbf{k}\|\sim k_F$ and $\|\mathbf{k}+\mathbf{q}\|\sim k_F$. Then, the number of solutions for $\mathbf{k}$ is optimal if $\|\mathbf{q}\|\sim 2k_F$. This solution corresponds to a triangular lattice of length $L_c=2\pi/(\sqrt{3}k_F)$ in real space leading to a unit cell of volume $\Omega_c=\sqrt{3}L_c^2/2$. Since the system is contained in the volume $\Omega=\sqrt{3}L^2/2$, we will obtain $N_c=\Omega_c/\Omega$ lattice sites or

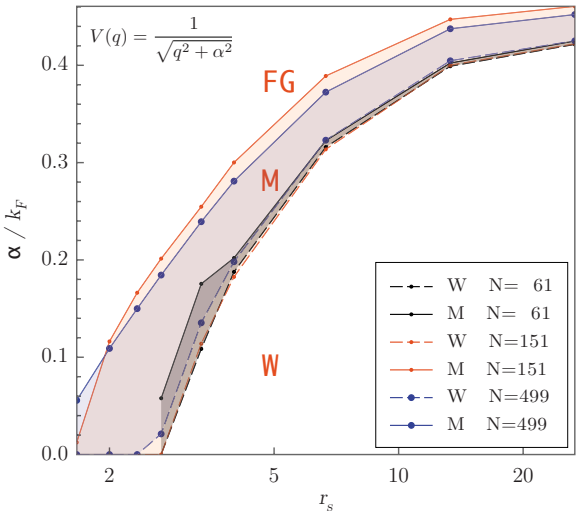

FIG. 4. (Color online) Effect of the screening on the ground-state phase diagram for $N=61$, 151, and 499. The different phases are labeled "FG" (Fermi-gas ground state), "M" (metallic ground state), and "W" (Wigner crystal). For all values of the screening parameter α of the screened Coulomb potential $V(q)$, we have found a metallic phase of energy lower than the Fermi gas and the Wigner crystal energy.

$$N_c = \frac{2\sqrt{3}}{\pi}N \approx 1.1N, \tag{2}$$

where we have used $n=N/\Omega=k_F^2/(4\pi)$. We will elaborate this argument into an analytical proof of an upper bound on the ground-state energy in Sec. V.

Numerically, it is possible to extend the Hartree-Fock study for models which differ from the pure electron gas. In order to check the stability of the metallic phase with respect to a modification of the singular Coulomb potential, we have performed calculations using a screened Coulomb potential. In Fig. 4 we show the ground-state phase diagram for three different system sizes. We see that for intermediate densities the metallic state remains the ground state of the finite sized system even in the presence of screening.

III. DESCENT METHOD

In this section we provide some details about the descent method used to obtain numerically the HF ground states of the electron gas. The variation of the total energy $\mathcal{E}(\psi_1,\psi_2,\ldots,\psi_N)$ with respect to a variation of the single-particle state $\delta\psi_i$ is given by

$$\delta\mathcal{E} = \sum_i \langle h_\Psi\psi_i|\delta\psi_i\rangle + \sum_i \langle\delta\psi_i|h_\Psi\psi_i\rangle, \tag{3}$$

where h_Ψ, the so-called HF Hamiltonian, is a single-particle operator depending on the full state Ψ (not on the particular choice of the ψ_i's). Extremal states must satisfy the following equation:

$$h_\Psi \psi_i = \sum_j C_{ij} \psi_j, \tag{4}$$

where C_{ij} are the Lagrange coefficients associated with the normalization constraint $\langle \psi_i | \psi_j \rangle = \delta_{ij}$. Conversely, if $\Psi = \psi_1 \wedge \cdots \wedge \psi_N$ is not an extremum, we have

$$h_\Psi \psi_i = \sum_j C_{ij} \psi_j + \theta_i, \tag{5}$$

where the θ_i's satisfy $\langle \psi_i | \theta_j \rangle = 0$, $\forall i,j$. Within the steepest-descent method one chooses first a $N \times N$ unitary transformation $A = (a_{ij})$ such that one obtains

$$\langle \psi_i' | \psi_j' \rangle = \delta_{ij}, \quad \langle \psi_i' | \theta_j' \rangle = 0, \quad \langle \theta_i' | \theta_j' \rangle = \|\theta_i\|^2 \delta_{ij} \quad \forall\, i,j \tag{6}$$

for the transformed single-particle states $\theta_i' = \Sigma_j a_{ij} \theta_j$, $\psi_i' = \Sigma_j a_{ij} \psi_j$. The energy $\mathcal{E}(\psi_1 + \lambda\theta_1, \ldots, \psi_N + \lambda\theta_N)$ can be expressed as a sum of rational fractions whose numerators and denominators are polynomials of order 4 at most: setting $\nu_i^2 = \|\psi_i' + \lambda\theta_i'\|^2 = 1 + \lambda^2 \|\theta_i'\|^2$ and $\chi_i = \psi_i' + \lambda\theta_i'$, we have

$$\begin{aligned} \mathcal{E}(\psi_1 + \lambda\theta_1, \ldots, \psi_N + \lambda\theta_N) &= \mathcal{E}(\chi_1/\nu_1, \ldots, \chi_N/\nu_N) \\ &= \sum_i \frac{1}{\nu_i^2} \langle \chi_i | -\Delta | \chi_i \rangle \\ &\quad + \sum_{i<j} \frac{1}{\nu_i^2 \nu_j^2} \langle \chi_i \wedge \chi_j | V | \chi_i \wedge \chi_j \rangle \\ &= \sum_i \frac{P_i^{(2)}}{\nu_i^2} + \sum_{i<j} \frac{P_{ij}^{(4)}}{\nu_i^2 \nu_j^2}, \end{aligned} \tag{7}$$

where $P_i^{(2)}$ (respectively, $P_{ij}^{(4)}$) are polynomials of order 2 (respectively, 4) in λ. Thus, it is possible to find the best λ and to iterate the process until a stationary state is reached.

In fact, this method has the same drawbacks as the steepest decent method in linear optimization problems; in general, it converges slowly. For linear problems, conjugate gradient methods are preferable.[13,14] However, since the HF states do not form a linear space, the genuine conjugate gradient method does not apply here. We have therefore adapted a variant of this method to the nonlinear case. Let η_i be the previous variation $\delta\psi_i$, and θ_i is obtained by Eq. (5). We then compute $\mathcal{E}(\psi_1 + \lambda\theta_1 + \mu\eta_1, \cdots, \psi_n + \lambda\theta_N + \mu\eta_N)$ for six values of the pairs $\{\lambda, \mu\}$ in order to approximate $\mathcal{E}$ by a polynomial of order 2 in λ and μ. Minimizing the polynomial with respect to λ and μ, we obtain the new changes of the single-particle states, $\delta\psi_i$, and the corresponding energy change. This process is iterated until the relative variation of the energy, $\delta\mathcal{E}/\mathcal{E}$, is sufficiently small.

We compute the wave function on a $N_g \times N_g$ grid, the fast Fourier transform is used to switch between real and reciprocal spaces.[15] We have systematically checked the convergence of the solution with respect to the grid size. For the FG ground state, convergence is reached once all k vectors up to $2k_F$ are represented in the grid ($N_g \sim 4\sqrt{N/\pi}$). At larger r_s, in the WC phase, the wave functions are essentially Gaussians.[16] The width δ of the Gaussians scales as $\delta/L \propto (r_s N)^{-1/2}$. For a correct resolution of the Gaussians we need $L/N_g \propto \delta$, so that the number of grid points increases at low densities, $N_g \propto (N r_s)^{1/2}$. Convergence is reached for $N_g = 32$ (respectively, 64, 128) for $N \leq 43$ (respectively, $N \leq 200$, $N \leq 500$) up to $r_s = 30$. Whenever the number of grid points is chosen too small, solutions without any particular symmetries are obtained.

We have further studied the influence of the initial state on the final solution by choosing different types of wave function for initialization: a WC state, a converged state stored at larger or lower r_s, a state initialized with random numbers, or a "metallic state" as described above.

Typically, the energies decrease exponentially with the number of iterations. The decrease in energy during transitions to a different symmetry is in general much smaller than the convergence within the same symmetry. We have often seen energy plateaus with changes of relative energy $\lesssim 10^{-4}$ just before the occurrence of a transition to a completely different state. For system sizes up to $N = 151$, the minimization is continued until a relative precision of 10^{-12} is reached, and for larger N a relative precision of 10^{-5} is used.

IV. ENERGY OF THE POLARIZED ELECTRON GAS FOR A SLATER STATE

In this section we set our notations and recall the basic formulas of the electron gas. We consider the Hamiltonian of N electrons in a 2D or three-dimensional (3D) square box of volume Ω with periodic boundary conditions

$$H = -\frac{\hbar^2}{2m}\Delta + \frac{e^2}{2}V, \tag{8}$$

where V is the two-body Coulomb potential $\Sigma_{i \neq j} 1/|r_i - r_j|$, the electron mass is m, and e is its charge. It is convenient to choose Hartree as the unit of energy, $Ha = \hbar^2/(m a_B^2)$. We get

$$H = \frac{a_B^2}{2}\left(-\Delta + \frac{1}{a_B} V \right). \tag{9}$$

Let ψ_n be an orthonormalized set of N vectors of $L^2(\Omega)$. They define the N-particle Slater determinant $\Psi = \wedge_n \psi_n$. Moreover, the energy of Ψ is

$$\mathcal{E} = \langle \Psi | H | \Psi \rangle = \frac{a_B^2}{2}\left(-\sum_n \langle \psi_n | \Delta | \psi_n \rangle + \frac{1}{a_B} \sum_{n,n'} \langle \psi_n \wedge \psi_{n'} | v | \psi_n \wedge \psi_{n'} \rangle \right), \tag{10}$$

where v is defined as

$$\langle \varphi_1 \otimes \varphi_2 | v | \psi_1 \otimes \psi_2 \rangle = \int dx dy \overline{\varphi_1}(x) \overline{\varphi_2}(y) \frac{1}{\|x - y\|} \psi_1(x) \psi_2(y). \tag{11}$$

In order to avoid problems due to the Coulomb singularity, we introduce the jellium model and define the potential acting on the plane waves ϕ_k as

$$\langle \phi_k \otimes \phi_{k'} | v | \phi_{k+q} \otimes \phi_{k'-q} \rangle = \frac{\pi}{\Omega} \left(\frac{2}{|q|} \right)^{D-1} \tag{12}$$

for $q \neq 0$ and 0 otherwise, so that the total charge of the electrons is compensated by a positive background charge.

The Fermi gas is defined by $\Phi = \wedge_{|k|<k_F} \phi_k$, where $(\alpha_D k_F)^D = (2\pi)^D N/\Omega$ and α_D^D is the volume of the unit sphere

$$\mathcal{E}_{\mathrm{FG}} = \langle \Phi | H | \Phi \rangle = \frac{a_B^2}{2} \left(\sum_{|k|<k_F} k^2 - \frac{2^{D-1}\pi}{a_B \Omega} \sum_{|k|,|k'|<k_F} \frac{1}{|k-k'|^{D-1}} \right). \tag{13}$$

As Ω goes to ∞ with Ω/N fixed, the thermodynamic limit for the energy per particle is obtained by the substitution $\Sigma_k \to \frac{\Omega}{(2\pi)^D} \int dk$,

$$\begin{aligned} \frac{\mathcal{E}_{\mathrm{FG}}}{N} &= \frac{a_B^2}{2} \frac{\Omega}{N(2\pi)^D} \left(\int_{|k|<k_F} dk k^2 \right. \\ &\quad \left. - \frac{1}{a_B 2\pi^{D-1}} \int_{|k|,|k'|<k_F} dk dk' \frac{1}{|k-k'|^{D-1}} \right) \\ &= \frac{a_B^2}{2} \frac{\Omega}{N(2\pi)^D} k_F^{D+2} \left(\int_{|k|<1} dk k^2 \right. \\ &\quad \left. - \frac{1}{a_B k_F 2\pi^{D-1}} \int_{|k|,|k'|<1} dk dk' \frac{1}{|k-k'|^{D-1}} \right). \end{aligned} \tag{14}$$

From the definition of $r_s = (\alpha_D a_B n^{1/D})^{-1}$ and k_F, it follows that $k_F \alpha_D^2 r_s a_B = 2\pi$. Thus, we have

$$\frac{\mathcal{E}_{\mathrm{FG}}}{N} = \frac{2\pi^2}{\alpha_D^{D+4} r_s^2} \left(\int_{|k|<1} dk k^2 - \frac{r_s \alpha_D^2}{4\pi^D} \int_{|k|,|k'|<1} dk dk' \frac{1}{|k-k'|^{D-1}} \right), \tag{15}$$

which gives for $D=2$ ($\alpha_2^2 = \pi$),

$$\frac{\mathcal{E}_{\mathrm{FG}}}{N} = \frac{2}{\pi r_s^2} \left(\int_{|k|<1} dk k^2 - \frac{r_s}{4\pi} \int_{|k|,|k'|<1} dk dk' \frac{1}{|k-k'|} \right). \tag{16}$$

V. HARTREE-FOCK UPPER BOUNDS FOR THE POLARIZED 2D ELECTRON GAS

In this section we estimate the energy for a class of states inspired by our numerical results. Let us consider a state $\Psi = \wedge_{|k|<k_F} \psi_k$, where

$$\psi_k = a_k \phi_k + b_k \phi_{k+Q_k}, \tag{17}$$

with Q_k in $\{-2k_F(\cos p\pi/3, \sin p\pi/3)\}_{p=0\ldots5}$. For $k = |k|(\cos\theta, \sin\theta)$ we choose Q_k such that $|k+Q_k|$ is minimal; that is, we choose p as the integer part of $(3\theta/\pi + 1/2)$ and we must assume b_k is zero if k is zero or $\theta = \pi/6 + n\pi/3$.

Furthermore, we assume that a_k and b_k are real positive number and invariant thru the rotation of $2n\pi/6$ and the symmetry $\theta \to -\theta$ (i.e., the dihedral group D_6). The ψ_k's are normalized, so that $a_k^2 + b_k^2 = 1$ and $b_k = 0$ if $|k \cdot Q_k| < 2k_F^2(1-\epsilon)$ (i.e., b_k is not zero only in the vicinity of $\{k_F(\cos p\pi/3, \sin p\pi/3)\}_{p=0\ldots5}$) (see Fig. 5).

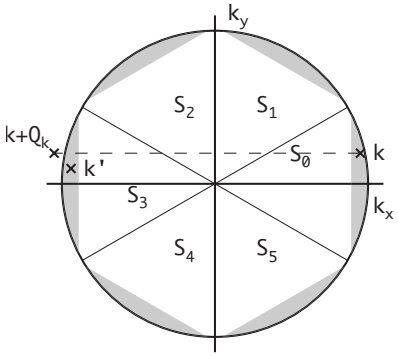

FIG. 5. The circle is the Fermi surface. The shaded surfaces are the regions where $b(k)$ is nonzero. The new state ψ_k mixing ϕ_k and ϕ_{k+Q_k} is now resonant with $\psi_{k'}$.

Thus, from Eqs. (10) and (17), the limit energy per particle is given by

$$\frac{\mathcal{E}}{N} = \frac{2}{\pi r_s^2} \left(\int_{|k|<1} dk \langle \psi_k | -\Delta | \psi_k \rangle + \frac{r_s}{4\pi} \int_{|k|,|k'|<1} dk dk' \frac{\Omega}{2\pi} \langle \psi_k \wedge \psi_{k'} | v | \psi_k \wedge \psi_{k'} \rangle \right), \tag{18}$$

where, as in Eq. (16), the k's have been renormalized by k_F and thus $|Q_k| = 2$.

We define ΔE by

$$\frac{\mathcal{E} - \mathcal{E}_{\mathrm{FG}}}{N} = \frac{2}{\pi r_s^2} \Delta E. \tag{19}$$

Then

$$\Delta E = \int_{|k|<1} dk [\langle \psi_k | -\Delta | \psi_k \rangle - k^2] + \frac{r_s}{4\pi} \Delta E_V, \tag{20}$$

where

$$\Delta E_V = \int_{|k|,|k'|<1} dk dk' \left(\frac{\Omega}{2\pi} \langle \psi_k \wedge \psi_{k'} | v | \psi_k \wedge \psi_{k'} \rangle + \frac{1}{|k-k'|} \right). \tag{21}$$

A. Potential-energy contribution: ΔE_V

Setting $v_q = 1/|q|$,

$$\begin{aligned} \frac{\Omega}{2\pi} \langle \psi_k \wedge \psi_{k'} | v | \psi_k \wedge \psi_{k'} \rangle + v_{k-k'} &= (v_{k-k'} - v_{k-k'-Q_{k'}}) b_{k'}^2 a_k^2 \\ &+ (v_{k-k'} - v_{k+Q_k-k'}) b_k^2 a_{k'}^2 + (v_{k-k'} - v_{k+Q_k-Q_{k'}-k'}) b_k^2 b_{k'}^2 \\ &+ 2 v_{Q_k} a_k b_k a_{k'} b_{k'} (\delta_{Q_k+Q_{k'}} + \delta_{Q_k-Q_{k'}}) \\ &- 2 v_{k-k'} a_k b_k a_{k'} b_{k'} \delta_{Q_k-Q_{k'}} - (v_{k+Q_k-k'} \\ &+ v_{k-k'-Q_{k'}}) a_k a_{k'} b_k b_{k'} \delta_{Q_k+Q_{k'}}. \end{aligned} \tag{22}$$

Equation (21) may be divided into four parts:

(i) $\{b_{k'}=0,\ b_k=0\}$: the contribution is zero.

(ii) $\{b_{k'}=0,\ b_k\neq 0\}$, $\{b_{k'}\neq 0,\ b_k=0\}$: both cases are equivalent.

For $\{b_{k'}=0,\ b_k\neq 0\}$, the integrant of Eq. (21) is

$$\frac{\Omega}{2\pi}(\psi_k\wedge\phi_{k'},v\psi_k\wedge\phi_{k'})+\frac{1}{|k-k'|}=(v_{k-k'}-v_{k+Q_k-k'})b_k^2. \tag{23}$$

Let S_0 be the sector of unit disk between $-\pi/6$ and $\pi/6$ (see Fig. 5); then in this sector $Q_k=(-2,0)$ and by symmetry

$$\int_{b_{k'}=0} dkdk'(v_{k-k'}-v_{k+Q_k-k'})b_k^2=6\int_{k\in S_0,b_{k'}=0} dkdk'(v_{k-k'}-v_{k+Q_k-k'})b_k^2, \tag{24}$$

$$=6\int_{k\in S_0,b_{k'}=0} dkdk'(v_{k-k'}-v_{\tilde{k}-k'})b_k^2, \tag{25}$$

$$\leq C\epsilon^3+6\int_{k\in S_0,|k_x'|<1-\epsilon} dkdk'(v_{k-k'}-v_{\tilde{k}-k'})b_k^2, \tag{26}$$

where $\tilde{k}=(2-k_x,k_y)$. In S_0, $k=(k_x,k_y)$ where k_x is close to 1 and setting $k_x=1-x$, we assume from now that $b_k=b(x/\epsilon)$.

In Appendix A, we prove that

$$\int_{k\in S_0,|k_x'|<1-\epsilon} dkdk'(v_{k-k'}-v_{k+Q_k-k'})b_k^2\leq 8\epsilon^2\sqrt{2\epsilon}[\ln\epsilon^{-1}+O(1)]\int_0^1 dxb^2(x)x\sqrt{x}. \tag{27}$$

(iii) $\{b_{k'}\neq 0,\ b_k\neq 0\}$: By symmetry we can assume that k belongs to S_0. If $k'\notin S_0\cup S_3$ all the v appearing in Eq. (22) are uniformly bounded. Moreover, since the k volume for each sector goes like $\epsilon\sqrt{\epsilon}$, the contribution of these terms is bounded by $C\epsilon^3$. In the same way $v_{k-k'}$ is bounded when $k\in S_3$ and $v_{k+Q_k-k'}$ is bounded when $k'\in S_0$. Thus setting

$$f:=a_k^2b_{k'}^2+b_k^2a_{k'}^2-2a_ka_{k'}b_kb_{k'}=(a_kb_{k'}-b_ka_{k'})^2, \tag{28}$$

$$g:=a_k^2b_{k'}^2+b_k^2a_{k'}^2+2a_ka_{k'}b_kb_{k'}=(a_kb_{k'}+b_ka_{k'})^2, \tag{29}$$

one can check that

$$\int_{b_kb_{k'}\neq 0}\frac{\Omega}{2\pi}\langle\psi_k\wedge\psi_{k'}|v|\psi_k\wedge\psi_{k'}\rangle+v_{k-k'}\leq C\epsilon^3+6\int_{k,k'\in S_0} dkdk'(v_{k-k'}f-v_{k+Q_k+k'}g). \tag{30}$$

In Appendix B we prove that

$$\int_{k,k'\in S_0} dkdk'(v_{k-k'}f-v_{k+Q_k+k'}g)\leq 4\epsilon^2\sqrt{2\epsilon}[\ln\epsilon^{-1}+O(1)]\int_0^1 dx\sqrt{x}\int_x^1 dx'[f(\epsilon x,\epsilon x')-g(\epsilon x,\epsilon x')]. \tag{31}$$

Thus, summing the four contributions gives

$$\Delta E_V\leq C\epsilon^3+6\epsilon^2\sqrt{2\epsilon}[\ln\epsilon^{-1}+O(1)]\int_0^1 dx\sqrt{x}\left\{16b^2(x)x+4\int_x^1 dx'[f(x,x')-g(x,x')]\right\}. \tag{32}$$

B. Kinetic-energy contribution

The variation of the kinetic energy is given by

$$\int_{|k|<1} dk[\langle\psi_k|-\Delta|\psi_k\rangle-k^2]=6\int_{k\in S_0} dk(\langle\psi_k|-\Delta|\psi_k\rangle-k^2), \tag{33}$$

$$=6\int_0^\epsilon dx\ 2y_m\ 4xb^2(x/\epsilon), \tag{34}$$

$$\leq 6\times 8\epsilon^2\sqrt{2\epsilon}\int_0^1 dx\sqrt{x}xb^2(x). \tag{35}$$

C. Total energy

Inserting Eqs. (32) and (35) in Eq. (20), the variation of the total energy from the Fermi-gas energy becomes

$$\Delta E\leq 6\epsilon^2\sqrt{2\epsilon}\int_0^1 dx\sqrt{x}\left(8xb^2(x)+\frac{r_s}{4\pi}[\ln\epsilon^{-1}+O(1)]\times\left\{16b^2(x)x+4\int_x^1 dx'[f(x,x')-g(x,x')]\right\}\right)=6$$
$$\times 8\epsilon^2\sqrt{2\epsilon}\int_0^1 dx\sqrt{x}\left(xb^2(x)+\frac{r_s}{2\pi}[\ln\epsilon^{-1}+O(1)]\times\left\{b^2(x)x-a(x)b(x)\int_x^1 dx'\ a(x')b(x')]\right\}\right). \tag{36}$$

Let us set

$$\delta=\epsilon^2\sqrt{\epsilon}, \tag{37}$$

$$I_1=\int_0^1 dx\sqrt{x}xb^2(x), \tag{38}$$

$$I_2=\frac{1}{5\pi}\int_0^1 dx\sqrt{x}\left[-b^2(x)x+a(x)b(x)\int_x^1 dx'a(x')b(x')\right]. \tag{39}$$

Then

$$\Delta E \leq 6 \times 8\sqrt{2}\delta\{I_1 - r_s I_2[\ln\ \delta^{-1} + O(1)]\}. \quad (40)$$

If $I_2 > 0$, as r_s goes to 0, ΔE is minimal in Eq. (40) for δ defined by

$$\delta_{\min} = \frac{1}{e}\exp\left(-\frac{I_1}{I_2 r_s}\right), \quad (41)$$

and finally inserting $\delta_{\min}$ in Eq. (40) gives

$$\Delta E \lesssim -\frac{6 \times 8\sqrt{2}}{e}\exp\left(-\frac{I_1}{I_2 r_s}\right) r_s I_2. \quad (42)$$

We now have to find a solution $b(x)$ such that I_2 is positive. Choosing $b(x)=b_0$ or $b(x)=b_0(1-x)$ leads to negative $I2$. In Appendix C, as r_s goes to 0 we find a family of b leading to

$$\Delta E \lesssim -r_s \exp\left(-\frac{5\pi}{3r_s} + \frac{O(1)}{\sqrt{r_s}}\right). \quad (43)$$

Though such a bound is correct in the thermodynamic limit for $r_s \to 0$, this behavior in not so relevant for finite systems. Our numerical calculations of Sec. II consider about 10^3 electrons where the uniform Fermi gas remains the ground state for $r_s \lesssim 1$. Thus the asymptotic bound (43) is not very helpful in comparing with our numerical results obtained for $r_s \approx 1$.

Nevertheless, for finite r_s, one can choose a suitable function b and evaluate numerically I_1 and I_2. For instance, with $b=b_\eta$ as in Eq. (C10) and $\eta=0.001$ we get

$$\frac{\mathcal{E} - \mathcal{E}_{\mathrm{FG}}}{N} \lesssim -2. \times 10^{-4} r_s^{-1} \exp\left(-\frac{18.5}{r_s}\right). \quad (44)$$

We can also understand why the metallic phase does not necessarily appear in small sized systems. For finite systems of N electrons, one must have at least one plane wave in the shaded region of Fig. 5: $|k \cdot Q_k| > 2k_F^2(1-\epsilon)$. This gives the condition $N\epsilon\sqrt{\epsilon} > 1$ and using Eqs. (37) and (41), this leads $N > \exp(3I_1/5I_2 r_s)$. Analogous to Eq. (43), we obtain the following lower bound:

$$N > \exp\left(\frac{3\pi}{r_s}\right), \quad (45)$$

i.e., $N > 500$ for $r_s = 1.8$. This bound is compatible with our numerical simulations where the metallic phase disappears at $r_s = 1$ for $N = 500$ and may explain why the metallic phase has not been observed in previous numerical calculations.

VI. CONCLUSION

Using a descent algorithm, we have computed the ground state of up to $N=500$ electrons. For $1 \lesssim r_s \lesssim 3$, our solutions have lower energies than the FG or WC. These solutions correspond to denser lattices that the WC solutions, that is, with less than one electron per site as in a metallic material.

We have proven, in the thermodynamic limit, that for sufficiently small r_s, these metallic states have always a smaller energy than the Fermi gas. We have demonstrated that the FG is not the ground state even at small r_s.

Our proof relies on the behavior at infinity of the Coulomb potential, so it may be interesting to check the existence of these states in the case of a screened Coulomb potential. A rigorous extension of our proof is not straightforward. However, as shown in Fig. 4, our numerical calculations indicate that the metallic phase persists in the presence of screening, at least for various system sizes and screening parameters studied. Thus, such metallic states should be considered as relevant candidates for further studies beyond the Hartree-Fock approximation, since, qualitatively, correlation effects amount to an effective screening of the electron interaction in the high-density limit.

ACKNOWLEDGMENTS

We thank J. Trail and R. Needs for providing us numerical data of Ref. 8 shown in Fig. 1. We thank D. Ceperley for discussions.

APPENDIX A

We have to estimate

$$I(f) = \int_{\substack{\|k\|,\|k'\| \leq 1 \\ 1-k_x < \epsilon, |k'_x| < 1-\epsilon}} dk dk' (v_{k-k'} - v_{\tilde{k}-k'}) f(1-k_x), \quad (A1)$$

where $\tilde{k}=(2-k_x,k_y)$ and f is a positive function. We have

$$\int dk'(v_{k-k'} - v_{\tilde{k}-k'}) = \int dk'_x \ \mathrm{arcsinh}\frac{y'_m - k_y}{k_x - k'_x} + \mathrm{arcsinh}\frac{y'_m + k_y}{k_x - k'_x} - \mathrm{arcsinh}\frac{y'_m - k_y}{2 - k_x - k'_x} - \mathrm{arcsinh}\frac{y'_m + k_y}{2 - k_x - k'_x}, \quad (A2)$$

where $y'_m = \sqrt{1-k'^2_x}$. Moreover, since $\mathrm{arcsinh}\, x - \mathrm{arcsinh}\, y \leq \ln x/y$ for $x > y > 0$,

$$\int dk'(v_{k-k'} - v_{\tilde{k}-k'}) \leq \int_{-1+\epsilon}^{1-\epsilon} dk'_x 2 \ln\frac{2 - k_x - k'_x}{k_x - k'_x}. \quad (A3)$$

We set $k_x = 1-x$ and $y_m = \sqrt{2x-x^2}$,

$$I(f) \leq \int_0^\epsilon dx f(x) 2 y_m \int_{-1+\epsilon}^{1-\epsilon} dk'_x 2 \ln\frac{1 + x - k'_x}{1 - x - k'_x}, \quad (A4)$$

$$= 4\int_0^\epsilon dx f(x) y_m \int_\epsilon^{2-\epsilon} du \ln\frac{u+x}{u-x}, \quad (A5)$$

$$\leq 4\int_0^\epsilon dx f(x) y_m \int_\epsilon^{2-\epsilon} du \frac{2x}{u-x}, \quad (A6)$$

$$= 8\epsilon^2\sqrt{2\epsilon}[\ln\ \epsilon^{-1} + O(1)]\int_0^1 dx f(\epsilon x) x\sqrt{x}. \quad (A7)$$

APPENDIX B

We have to estimate

$$I(f,g)=\int_{\substack{\|k\|,\|k'\|\le 1\\ 1-k_x,1-k'_x<\epsilon}} dkdk'(v_{k-k'}f-v_{\tilde{k}+k'}g), \tag{B1}$$

where $\tilde{k}=(k_x-2,k_y)$ and f and g are positive functions of $1-k_x$ and $1-k_{x'}$. Setting $k_x=1-x$, $k'_x=1-x'$, $k_y=y$, $k'_y=y'$, and $r_\pm=\sqrt{(x\pm x')^2+(y-y')^2}$, Eq. (B1) can be rewritten as

$$I(f,g)=\int_0^\epsilon dx\int_0^\epsilon dx'\int dydy'\left(\frac{1}{r_-}f-\frac{1}{r_+}g\right)$$

$$=2\int_0^\epsilon dx\int_x^\epsilon dx'\int dydy'\left(\frac{1}{r_-}f-\frac{1}{r_+}g\right), \tag{B2}$$

where y and y' must satisfy $(1-x)^2+y^2\le 1$ and $(1-x')^2+y'^2\le 1$.

Since $\operatorname{arcsinh} x\le \ln 2(x+1)$, the first term in Eq. (B2) is bounded by

$$2\int_0^\epsilon dx\int_x^\epsilon dx'\int dydy'\frac{1}{r_-}f=2\int_0^\epsilon dx\int_x^\epsilon dx'f\int_{-y_m}^{y_m}dy$$

$$\times\left(\operatorname{arcsinh}\frac{y'_m+y}{x'-x}+\operatorname{arcsinh}\frac{y'_m-y}{x'-x}\right), \tag{B3}$$

$$\le 2\int_0^\epsilon dx\int_x^\epsilon dx'f\int_{-y_m}^{y_m}dy\,2\operatorname{arcsinh}\frac{2y'_m}{x'-x}, \tag{B4}$$

$$\le 4\int_0^\epsilon dx\int_x^\epsilon dx'f\,2y_m\ln\left(2+\frac{4y'_m}{x'-x}\right), \tag{B5}$$

$$\le 4\epsilon^2\sqrt{2\epsilon}[\ln(\epsilon^{-1})+O(1)]\int_0^1 dx\int_x^1 dxf(\epsilon x,\epsilon x')\sqrt{x}. \tag{B6}$$

On the other hand, using $\operatorname{arcsinh} x\ge \ln 2x$, the last term of Eq. (B2) is

$$2\int_0^\epsilon dx\int_x^\epsilon dx'g\int dydy'\frac{1}{r_+}=2\int_0^\epsilon dx\int_x^\epsilon dx'g\int_{-y_m}^{y_m}dy$$

$$\times\operatorname{arcsinh}\frac{y'_m-y}{x+x'}+\operatorname{arcsinh}\frac{y'_m+y}{x+x'}, \tag{B7}$$

$$\ge 2\int_0^\epsilon dx\int_x^\epsilon dx'g\int_{-y_m}^{y_m}dy\,\ln 4\frac{y'^2_m-y^2}{(x+x')^2}, \tag{B8}$$

$$\ge 4\int_0^\epsilon dx\int_x^\epsilon dx'gy_m[\ln\epsilon^{-1}+O(1)], \tag{B9}$$

$$\ge 4\epsilon^2\sqrt{2\epsilon}[\ln\epsilon^{-1}+O(1)]\int_0^1 dx\int_x^1 dx'g(\epsilon x,\epsilon x')\sqrt{x}. \tag{B10}$$

Moreover, we have

$$I(f,g)\le 4\epsilon^2\sqrt{2\epsilon}[\ln\epsilon^{-1}+O(1)]\int_0^1 dx\sqrt{x}\int_x^1 dx'[f(\epsilon x,\epsilon x')-g(\epsilon x,\epsilon x')]. \tag{B11}$$

APPENDIX C

Here we provide exact bounds on I_1 and I_2 given by Eqs. (38) and (39). In order to estimate I_2 we introduce the linear operator A,

$$Af(x)=\frac{1}{2x}\int_x^1 f(y)dy+\frac{1}{2x\sqrt{x}}\int_0^x f(y)\sqrt{y}dy, \tag{C1}$$

defined on the Hilbert space of the functions on [0,1] with the scalar product

$$\langle f|g\rangle=\int_0^1 x\sqrt{xf(x)}g(x)dx. \tag{C2}$$

Then A is a bounded symmetric operator and

$$I_2/I_1=\frac{1}{5\pi}\left(\frac{\langle ab|Aab\rangle}{\|b\|^2}-1\right). \tag{C3}$$

The unitary operator $f(x)\to g(y)=f(e^{-y})e^{-5/4y}$ from $L^2([0,1],x\sqrt{x}dx)$ onto $L^2([0,+\infty],dx)$ maps the operator A onto the operator $\tilde{A}$,

$$\tilde{A}g(x)=\frac{e^{-x/4}}{2}\int_0^x e^{y/4}g(y)dy+\frac{e^{x/4}}{2}\int_x^{+\infty}e^{-y/4}g(y)dy. \tag{C4}$$

Then

$$\tilde{A}e^{ikx}=\frac{1}{4(1/16+k^2)}e^{ikx}-\frac{1}{1/2+i2k}e^{-x/4}, \tag{C5}$$

thus setting

$$g_k(x)=\frac{1}{|1+i4k|}[(1+i4k)e^{ikx}-(1-i4k)e^{-ikx}]. \tag{C6}$$

$\{g_k\}_{k>0}$ is a full set of pseudoeigenvectors satisfying

$$\tilde{A}g_k=\frac{1}{4(1/16+k^2)}g_k.$$

Thus the spectrum of $\tilde{A}$ is (0,4) and the spectral measure is purely absolutely continuous; the largest spectral value is 4 with a pseudoeigenvector $g_4(x)=x+4$ corresponding to $f_4(x)=x^{-5/4}(4-\ln x)$. But $\|f_4\|$ is infinite and f_4 diverges at 0. The next step is to choose a family of functions b_η such that $a_\eta=\sqrt{1-b_\eta}$ is defined and $\langle a_\eta b_\eta|Aa_\eta b_\eta\rangle/\|b_\eta\|^2$ is close to 4.

Thus setting $f_\eta(x)=\min[f_4(x),f_4(\eta)]$ for $0<\eta\ll 1$, we have

$$\|f_\eta\|^2 = -\frac{1}{3}\left[\ln^3\ \eta - \frac{66}{5}\ln^2\ \eta + O(\ln\ \eta)\right], \tag{C7}$$

$$\langle f_\eta|Af_\eta\rangle = -\frac{4}{3}\left[\ln^3\ \eta - \frac{41}{5}\ln^2\ \eta + O(\ln\ \eta)\right], \tag{C8}$$

Then

$$\frac{\langle f_\eta|Af_\eta\rangle}{\|f_\eta\|^2} = 4 - \frac{20}{|\ln\ \eta|} + O(\ln^{-2}\ \eta). \tag{C9}$$

Thus f_η is a good candidate for the linear part of the problem. Now, by the simple scaling

$$b_\eta(x) = \frac{f_\eta(x)}{\sqrt{2}f_\eta(\eta)}, \tag{C10}$$

we get the nonlinear candidate satisfying $b_\eta(x)\le 1/\sqrt{2}$, $a_\eta=\sqrt{1-b_\eta^2}$ is well defined, $a_\eta(x)\ge 1/\sqrt{2}$, and b_η satisfies Eq. (C9).

We must now estimate the simultaneous convergence of $I2/I1$ [Eq. (C3)] and I_2 as η decreases. We have

$$\begin{aligned}\langle b_\eta|Ab_\eta\rangle - \langle b_\eta a_\eta|Ab_\eta a_\eta\rangle &= -\langle b_\eta - b_\eta a_\eta|A|b_\eta - b_\eta a_\eta\rangle + 2\langle b_\eta - b_\eta a_\eta|A|b_\eta\rangle \le 2\langle b_\eta - b_\eta a_\eta|A|b_\eta\rangle \\ &= 8\langle b_\eta - b_\eta a_\eta|b_\eta\rangle + 2\langle b_\eta - b_\eta a_\eta|(A-4)b_\eta\rangle \le 8\langle b_\eta - b_\eta a_\eta|b_\eta\rangle \\ &\quad + 2\|b_\eta - b_\eta a_\eta\|\|(A-4)b_\eta\| \le 8\langle b_\eta - b_\eta a_\eta|b_\eta\rangle + 8\|b_\eta - b_\eta a_\eta\|\sqrt{\langle b_\eta|(A-4)b_\eta\rangle},\end{aligned}$$

where

$$\begin{aligned}\langle b_\eta - b_\eta a_\eta|b_\eta\rangle &= \int_0^1 b_\eta(x)^2[1-a_\eta(x)]x\sqrt{x}dx \\ &\le \int_0^1 b_\eta(x)^2[1-a_\eta(x)]^2 x\sqrt{x}dx\ \sup\frac{1}{1-a_\eta} \\ &\le \|b_\eta - b_\eta a_\eta\|^2\frac{\sqrt{2}}{\sqrt{2}-1},\end{aligned}$$

and since $b_\eta - b_\eta a_\eta > 0$,

$$\begin{aligned}\|b_\eta - b_\eta a_\eta\|^2 &= \|b_\eta\|^2 - \|b_\eta a_\eta\|^2 - 2\langle b_\eta - b_\eta a_\eta|b_\eta a_\eta\rangle \\ &\le \|b_\eta\|^2 - \|b_\eta a_\eta\|^2 = \|b_\eta^2\|^2.\end{aligned}$$

By a direct computation,

$$\|b_\eta^2\|^2 \le \|b_\eta\|^2\frac{6}{5|\ln\ \eta|}$$

for η small enough and thus

$$\frac{\langle b_\eta|Ab_\eta\rangle}{\|b_\eta\|^2} - \frac{\langle b_\eta a_\eta|Ab_\eta a_\eta\rangle}{\|b_\eta\|^2} \le \frac{8}{|\ln\ \eta|}\left(\frac{\sqrt{2}}{\sqrt{2}-1}\frac{6}{5} + 2\sqrt{6}\right). \tag{C11}$$

Finally, from Eq. (C9) for b_η and Eq. (C11) and $I_1=\|b_\eta\|^2$, Eq. (C3) gives

$$I_2/I_1 \ge \frac{1}{5\pi}\left(3 - \frac{C}{|\ln\ \eta|}\right) + O(\ln^{-2}\ \eta), \tag{C12}$$

$$I2 \le \frac{2}{15\pi}\eta^{5/2}|\ln^3\ \eta|\left[1 + O\left(\frac{1}{|\ln\ \eta|}\right)\right], \tag{C13}$$

where

$$C = 20 + 8\left(\frac{\sqrt{2}}{\sqrt{2}-1}\frac{6}{5} + 2\sqrt{6}\right) \approx 92. \tag{C14}$$

Choosing η sufficiently small, this proves that ΔE is strictly negative for any $r_s>0$; furthermore choosing η to minimize ΔE [Eq. (42)], i.e., $9r_s|\ln\ \eta|^2=2C\pi$, we obtain as r_s goes to 0:

$$\Delta E \le -r_s\exp\left(-\frac{5\pi}{3r_s} + \frac{O(1)}{\sqrt{r_s}}\right). \tag{C15}$$

[1] B. Tanatar and D. M. Ceperley, Phys. Rev. B **39**, 5005 (1989); C. Attaccalite, S. Moroni, P. Gori-Giorgi, and G. B. Bachelet, Phys. Rev. Lett. **88**, 256601 (2002).

[2] B. Bernu, L. Cândido, and D. M. Ceperley, Phys. Rev. Lett. **86**, 870 (2001).

[3] H. Falakshahi and X. Waintal, Phys. Rev. Lett., **94**, 046801 (2005); X. Waintal, Phys. Rev. B **73**, 075417 (2006).

[4] E. P. Wigner, Trans. Faraday Soc. **34**, 678 (1938); Phys. Rev.

46, 1002 (1934).
[5] A. W. Overhauser, Phys. Rev. Lett. **4**, 462 (1960); Phys. Rev. **128**, 1437 (1962).
[6] B. Spivak and S. A. Kivelson, Phys. Rev. B **70**, 155114 (2004).
[7] G. F. Giuliani and G. Vignale, *Quantum Theory of the Electron Liquid* (Cambridge University Press, Cambridge, 2005).
[8] J. R. Trail, M. D. Towler, and R. J. Needs, Phys. Rev. B **68**, 045107 (2003).
[9] S. Zhang and D. M. Ceperley, Phys. Rev. Lett. **100**, 236404 (2008).
[10] S. V. Kravchenko, G. V. Kravchenko, J. E. Furneaux, V. M. Pudalov, and M. D'Iorio, Phys. Rev. B **50**, 8039 (1994).
[11] S. Pankov and V. Dobrosavljević, Phys. Rev. B **77**, 085104 (2008); Physica B **403**, 1440 (2008).
[12] A. Camjayi, K. Haule, V. Dobrosavljević, and G. Kotliar, Nat. Phys. (unpublished).
[13] G. H. Golub and C. Van Loan, *Matrix Computations*, 2nd ed. (Johns Hopkins University Press, Baltimore, Maryland, 1989).
[14] F. Delyon and M. Duneau, J. Comput. Phys. **207**, 375 (2005).
[15] In reciprocal space, the k vectors of the WC fall on the grid.
[16] Indeed, a simple variational calculation with only one parameter, the width of the Gaussians, gives the HF energy with a relative precision better than 0.1%.